Accepted Manuscript

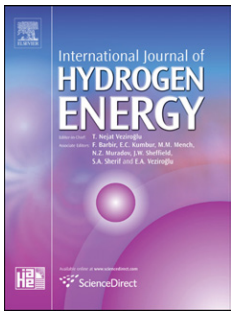

Plane hydrogen jets

D. Makarov, V. Molkov

PII: S0360-3199(13)00591-0

DOI: 10.1016/j.ijhydene.2013.03.017

Reference: HE 11452

To appear in: *International Journal of Hydrogen Energy*

Received Date: 1 August 2012

Revised Date: 28 February 2013

Accepted Date: 4 March 2013

Please cite this article as: Makarov D, Molkov V, Plane hydrogen jets, *International Journal of Hydrogen Energy* (2013), doi: 10.1016/j.ijhydene.2013.03.017.

PLANE HYDROGEN JETS

D. Makarov[1], V. Molkov

**Hydrogen Safety Engineering and Research Centre (HySAFER), University of Ulster
Newtownabbey, Co.Antrim, BT37 0QB, United Kingdom**

Abstract

This study is focused on understanding the structure and behaviour of hydrogen under-expanded jets from plane nozzles and their differences with circular nozzle jets. Results of numerical simulations of hydrogen highly under-expanded jets from a storage vessel at pressure 40 MPa through a circular nozzle and two plane nozzles with aspect ratios 5.0 and 12.8 respectively, all of the same cross-section area, are presented. Two stages approach is applied to simulate under-expanded unignited jets and jet fires. At the first stage, the high Mach number flow in a near field to the nozzle is simulated by compressible flow solver. At the second stage, incompressible flow solver is applied to simulated either unignited or combusting jets in the far from the nozzle field with "inner" boundary conditions taken from the first stage. The structure and behaviour of hydrogen plane highly under-expanded jets is scrutinised, including the switch-of-axis phenomenon when the exiting jet expands in the vicinity of the nozzle only in the direction of the minor nozzle axis while it contracts in the major axis direction. Simulations demonstrated that plane jets may provide faster concentration decay compared to axisymmetric jets with the same mass flow rate due to the difference in air entrainment. The concentration decay rate is shown to be a function of the plane nozzle aspect ratio. The eddy break-up model is applied to simulate under-expanded hydrogen jet fires from the equipment at pressure of 40 MPa. The circular and plane nozzle jet fire simulations are validated against experiments by Mogi and Horiguchi (2009). The simulations are in a good agreement with the experiment.

Keywords: hydrogen, high pressure, plane jet, underexpanded, CFD, separation distance

1 Introduction

The increasing use of hydrogen as an energy carrier requires the development of efficient safety strategies and engineering solutions for inherently safer design and exploitation of fuel cell and hydrogen (FCH) systems and infrastructure. The majority of various hydrogen early market applications rely on storage of hydrogen as compressed gas at pressure as high as 100 MPa. Permitting and land planning procedures require knowledge of deterministic separation distances. Due to high storage pressure the separation distances could be quite large that directly affects a cost of FCH system and/or infrastructure. There is a need in innovative engineering solutions that can reduce the separation distances for both hydrogen unignited releases and jet fires. Commission Regulation (EU) No 406/2010 of 26 April 2010 implementing Regulation (EC) No 79/2009 of the European Parliament and of the Council on type-approval of hydrogen-powered motor vehicles requires use of pressure relief devices (PRD) for on-board hydrogen storage. The efficient PRD, when triggered, should produce a jet fire of shortest possible flame length, if leak is ignited, or a flammable envelope of minimum size, if release is unignited. The need in significant reduction of deterministic separation distances causes a serious interest to the under-expanded jet control and, in particular, to the provision of quicker hydrogen concentration decay by using jets of different shape.

Plane nozzle flow is a realistic scenario when leaks are from high-pressure equipment cracks, fittings, etc. Nonetheless, safety strategies are often concentrated on analysis of behaviour of axisymmetric jets following an assumption that even for high-aspect ratio rectangular nozzles a concentration decay characteristic for

[1]Author for correspondence. Email: dv.makarov@ulster.ac.uk, tel: +44(0)2890368751, fax: +44(0)2890368726
Address: 27B06, University of Ulster, Shore Rd., Newtownabbey, Co.Antrim, BT370QB, UK.

axisymmetric jets will occur at some point downstream [1]. The validity of this assumption will be scrutinised in this paper. The overview of previous studies presented below includes the results for various gases as data on hydrogen jets is quite limited yet the behaviour of different plane jets could exhibit similarity.

1.1 Incompressible plane jets

First theoretical studies of laminar subsonic constant density jets in the absence of buoyancy are dated back to the beginning of last century, when Schlichting analysed analytically axisymmetric and two-dimensional (2D) plane laminar jets of constant density issued into a semi-infinite space [2]. The analytical 2D jet solution was improved later by Bickley [3]. Both are exact solutions of Prandtl's boundary layer equations and may be found in Schlichting's classical textbook [4]. The results show that compared to the infinitely long 2D plane jet the axisymmetric laminar jet, having the same diameter as 2D nozzle width, has larger entrainment potential, i.e. the axial concentration decay in an infinite plane (2D) jet is not as effective as in the axisymmetric jet.

For incompressible turbulent jets it is known [4] that the jet width for both axisymmetric and 2D nozzles is proportional to the distance from the nozzle x, though with different proportionality coefficients. This is based on the proportionality of the turbulent mixing length and the jet width. However, theoretically predicted decay of the centreline velocity u_{max} in the momentum-dominated turbulent axisymmetric jet is inversely proportional to the coordinate along jet axis, x^{-1}, while for the 2D jet it is inversely proportional to the square root from the distance, $x^{-0.5}$. The latter means that the entrainment to the axisymmetric turbulent jet from a nozzle of diameter D is more efficient to facilitate the axial concentration decay than the entrainment to the turbulent jet from the infinitely long plane slot of width D. Indeed, the axial velocity should decay faster when the entrainment is stronger. Analogous behaviour can be expected for the concentration decay in jets following the similarity of momentum and specie conservation equations.

In 1955 Vulis and Terekhina [5] studied axisymmetric turbulent jets in a large range of densities, including hydrogen jet released into air. They demonstrated analytically and experimentally that non-dimensional momentum profile in a jet cross section doesn't depend on the jet density and remains self-similar along the jet downstream axis. However, the smaller density of the released gas compared to the surrounding gas density, the faster the absolute velocity decay. This conclusion was confirmed experimentally by other authors [6], [7]. Thus, concentration decay in hydrogen jet issued into still air is expected to be faster compared to concentration decay of heavier gases, e.g. hydrocarbon gaseous fuels.

A comprehensive review of experimental data on velocity and species concentrations measurements in momentum- and buoyancy-dominated incompressible jets is published in 1980 by Chen and Rodi [8] for both plane and axisymmetric jets. The introduced scaling laws are in line with former theoretical predictions by Schlichting [4], and the similarity law by Ricou and Spalding [6]. Axial mass fraction of specie in the axisymmetric incompressible jet is correlated as $C/C_0 = 5.4(D/x)(\rho_N/\rho_S)^{0.5}$, where C is the axial mass fraction, C_0 is the mass fraction of specie in the nozzle, D is the nozzle diameter, x is the coordinate along the jet axis, ρ_N is the specie density in the nozzle, ρ_S is the density of the surrounding gas. Axial concentration decay in infinite plane (2D) jet is correlated as $C/C_0 = 2.13(D/x)^{0.5}(\rho_N/\rho_S)^{0.5}$, where D is the width of 2D nozzle. Unfortunately, validity limits of this correlation when used with finite length plane nozzles were not specified.

Probably the first study on turbulent jets from a finite aspect ratio (AR) rectangular nozzle was published by Van Der Hegge Zijnen in 1957 [9]. The isothermal incompressible flow of air from a sharp-edged nozzle AR=20 with Reynolds number 13,300 was investigated. The flow was studied in a near field up to 40 characteristic nozzle widths downstream. So-called "saddle-shape" velocity profile was observed in experiments, when the maximum velocity in a cross-section along the minor nozzle axis plane was located off the centreline, though a difference between the maximum and the centreline velocities was just 4%.

Later research aimed to study the flow in a far field downstream up to 400 characteristic nozzle widths [10],[11]. In 1966 Sforza et al. [10] studied turbulent incompressible (expanded) jets from rectangular sharp-edged nozzles having AR up to 40 and an elliptic nozzle with AR=9.35. A faster spreading rate of a jet in the minor axis direction of the nozzle compared to the spreading rate in its major axis direction was reported. It was identified that a typical jet structure consists of three regions: 1 – potential core region, where mixing initiated at jet boundaries don't yet permeate through the entire jet width, 2 – nearly two-dimensional or characteristic decay region, where the centreline velocity decay depends on nozzle configuration and the velocity decay in directions of major and minor axes is different, 3 – region of axisymmetric decay, where the velocity decay is axisymmetric in nature. The experimental results indicated that in a three-dimensional jet the major axis half-width initially decreases while the minor axis half-width grows. At some point jet widths in both directions become equal, i.e. graphs of widths cross each other. This location is called “crossover point”. Then both jet widths grow but at different rates. Finally jet widths approach each other in a far field downstream, and then the jet decays axisymmetrically.

In study [10] the crossover point coincides with the onset of the axisymmetric character of centreline (axial) velocity decay. It was found that the jet potential core length depends on the nozzle width, i.e. the smaller dimension, while the characteristic decay region length depends on the nozzle length, i.e. the longer dimension. Sforza et al. [10] also observed “saddle-shape” velocity profile, which extended from the potential core into the characteristic decay region. One year later, Trentacoste and Sforza expanded this research by the measurement of velocity profiles for elliptic and rectangular orifice-type nozzles [11], and detailed measurements of mass entrainment rate.

In 1979 Sfeir [12] studied plane incompressible air jets from rectangular nozzles of three different aspect ratios, namely10, 20, and 30. There were two nozzle inlet geometries, i.e. a sharp-edge rectangular orifice and a long channel, for each aspect ratio. He found that the shape of a nozzle entrance plays an important role in jet development, e.g. the crossover point appears further downstream for a jet emanating from a long channel than for a jet from a sharp-edged orifice-type nozzle.

A series of experiments with incompressible, subsonic compressible, and chocked under-expanded air jets with finite aspect ratio rectangular nozzles was conducted at Stanford in 1981-1982 [13]-[15]. The incompressible flow results were reported by Krothapalli et al. [13] for “long channel” type plane nozzles with AR=5.5, 8.3, 12.5 and 16.7 in a range of axial distance from the nozzle to nozzle width ratios up to 115. The study of rectangular nozzle jets demonstrated that the transition from the centreline velocity decay characteristic for 2D jets, i.e. $u \sim x^{-0.5}$, to decay in axisymmetric flow, i.e. $u \sim x^{-1}$, occurs the further downstream the larger AR.

In 1987 Shadow et al. [16] studied reacting subsonic jets of ethylene/oxygen/nitrogen mixture issued from elliptical nozzles with AR=2, 3 and 3.5 into co-flowing air. The most effective enhancement of fuel-air mixing and the shortest flame length was found not for the nozzle with the largest AR=3.5, but for the nozzle with AR=3.0. The authors suggested that the more intensive vortex activity, observed around the elliptic nozzle tip, increased fine-scale mixing and enhanced combustion near the nozzle.

1.2 Compressible subsonic and supersonic plane jets

In 1957 Crane and Pack [17] derived analytical solutions for compressible infinite plane (2D) and axisymmetric turbulent jets based on a number of simplifying assumptions. It was concluded that for 2D jets the compressibility effect increases the width of the mixing region and the spread rate. For axisymmetric jets the compressibility resulted in a narrower velocity profile as the speed rose. This result was confirmed experimentally in 1963 by Maydew and Reed [18] who investigated turbulent mixing of compressible axisymmetric air jets at Mach numbers up to *M*=1.96. They found that as a function of non-dimensional coordinate $\sigma y/x$, where σ is the constant, x is the coordinate along jet axis, and y is the coordinate transversal to jet axis, the velocity profile u/u_0, where u_0 is the nozzle exit velocity, and u is the gas velocity in the jet, is

essentially the same as for incompressible flow, but with the increase of Mach number the constant σ increases, i.e. the jet spreading rate decreases [18].

Subsonic compressible air jets were studied in 1982 by Hsia et al. [14] for the same nozzles as in their previous study [13], i.e. AR=5.5, 8.3, 12.5 and 16.7.The exit Mach number varied from 0.18 to 0.8. Subsonic compressible jets were found to behave qualitatively similar to the incompressible jets. The higher Mach number of subsonic flows led to the longer extension of the characteristic decay region, where velocity decays as $u \sim x^{-0.5}$.

The same nozzles as in [13] and [14] were used by authors to study under-expanded choked air flows [15]. Experiments were carried out using the pressure ratios 2.7, 3.8 and 5.8 with Mach numbers 1.3, 1.5 and 1.8 respectively. The complete flow axisymmetry was not found for the downflow distances studied up to x/D=160, where D is the nozzle width, though the centreline velocity was decaying as $u \sim x^{-1}$ from distances greater than x/D=80 for all three pressures (upstream of x/D=80 the velocity decayed as in the case of infinite plane jet, $u \sim x^{-0.5}$). The spreading rate in the minor axis was higher than that for incompressible flow. The axes switch: the major axis becomes the minor one, and vice versa. It was observed that the 2D type of the centreline velocity decay is retained after the switch of axes. The authors suggested that this "two dimensionality" of the jet will be preserved the longer downstream the larger the pressure ratio.

The highest rate of jet spread in minor axis was found at the pressure ratio 3.8 and not 5.8 [15]. It corresponded to the most intense generation of "screech sound", i.e. acoustic excitation of the entire jet flow field which serves to introduce large scale coherent wave structures increasing spreading rate of the jet. However, the increase of the pressure ratio in these tests led to decrease of the intensity of the acoustic excitation and as a sequence to decrease of the spreading rate.

In 1986 Gannochenko et al. [19] studied under-expanded plane air jets with nozzles aspect ratio up to AR=55.5.The ratio of nozzle exit to ambient pressures $n= p_N /p_S$ was up to 110. The study concentrated on location of central compression shock (CCS), which is a plane jet analogy to Mach disk in axisymmetric jets. Location of CCS of the jet, issued from the plane nozzle at pressure ratios $n=p_N /p_S$ more than 14, was close to location of CCS for jets from a round nozzle of the same cross section area. After n=80 location of CCSs for plane and axisymmetric jets practically coincided. Unfortunately, no information on jets' structure and further downstream jet behaviour were reported.

In 1989 Schadow et al. [20] studied the supersonic combustion-related shear flow dynamics of air jets from an elliptic nozzle of AR=3. In a non-reacting under-expanded elliptic air jet a series of bouncing expansion and compression waves generate a non-symmetric structure of cells with angles of oblique shocks and expansion fans that are different for two jet symmetry planes. The switch-of-axes in this supersonic flow occurred at distance of about 3 calibres (based on equivalent diameter of cross-sectional nozzle area) downstream, instead of about 20 calibres for subsonic jets.

In the same year Gutmark et al. [21] compared mixing characteristics of round, elliptic and rectangular jets for cold and hot air at subsonic (M=0.15), sonic (M=1.0), and supersonic (M=1.26 and M=1.5) velocities. The maximum nozzle to ambient pressure ratio was 3.8. Both elliptic and rectangular jets had a higher spreading rate compare to a round jet. The spreading rate in the minor axis of both subsonic and sonic jets is 50% higher than that of the major axis. However, when the jet becomes supersonic than the spreading rate along the minor axis is more than doubles relative to the subsonic jets and the spread at the major axis. The larger spread rate in minor axis for elliptic and rectangular nozzles weakens the shock cell structure. They also argued that the elliptic nozzle provided slightly faster mixing relative to the rectangular one, though the flow was studied just 30 equivalent nozzle diameters downstream. The saddle-shape velocity profile in the minor axis plane of the under-expanded jet in a close to nozzle field was also observed. In 1990 Gutmark et al. [22] extended study

supersonic jets to *M*=2.4 (pressure ratio 15), though it was focused on the near field (up to 30 equivalent diameters) pressure fluctuations interaction with the spread rate of the jet.

In 1998 further study of under-expanded jet flows from oval nozzles of AR=1.0, 1.4, 2.0, 2.9, and 5.0 was performed by Rajakuperan and Ramaswamy [23] in a pressure ratio range 2.3-20.3. They found that the higher pressure ratio increases the spreading rate in the minor axis, but has marginal effect on the spread rate in the major axis. Higher pressure ratio also corresponded to a shorter distance to location where jet widths in minor and major axes became equal, i.e. the crossover point or axis switching location, in the range of pressure ratios 7.0-20.3.

Detailed simulation of the jet from a rectangular nozzle with AR=8 and pressure ratio 50 was carried out as a model demonstration in 2008 by Usami et al. [24] in a near to the nozzle field. Presented velocity iso-lines in jet cross-sections show that the jet crossover distance is about 4-6 equivalent diameters downstream (based on the diameter of round nozzle with the same cross-section area).

In 2002 Wakes et al. [1] studied leakage from “damaged flange gaskets”. Different patterns of flange notches, representing various failed gaskets, were tested experimentally. Range of aspect ratios varied from AR=26.6 to 199.7, when measured at inner flange diameter, and from AR=26.6 to 239.5, when measured at outer flange diameter. The studied pressure ratios were in the range from 1.68 to 5.08. The behaviour of jet widths in minor and major axes for different notch patterns had different tendencies and difficult to generalise. Notches with radial cuts in gaskets tended to have spreading angle in minor axis plane larger than in the major axis and increasing with growing pressure, while spreading angle in major axis was decreasing with pressure. The highest spread rate was obtained for the leak with highest AR. It was observed that for the higher pressures the potential core length decreases significantly compare to axisymmetric one. The centreline velocity decay for the studied gasket notches is reported, but unfortunately without data on mass flow rates or gas velocities at the nozzle exit.

In 2009 Mogi and Horiguchi [25] performed under-expanded hydrogen jet fires experiments. Three nozzles of the same cross-section area were used: one round nozzle of 1 mm diameter and two rectangular nozzles with AR=5 and AR=12.8 respectively. The spouting pressure was 40 MPa. The jet flame length was found to decreases with the increase of AR. Indeed, the axisymmetric jet fire provided flame length of about 4.5 m, while plane jet fire lengths were 2.5 m and 2.2 m for AR=5 and AR=12.8 respectively. As the research was aimed at hazards of hydrogen jet flames, neither information on plane nozzle jet structures in the near field was given, nor physical mechanisms of flame decrease were discussed.

1.3 The switch-of-axes phenomenon

The switch-of-axes phenomenon was reported in a number of papers. In particular, the dependence of jet spreading rate on experimental parameters was discussed. The role of closed vortex rings surrounding the plane subsonic jet as it develops was first mentioned, probably, by Van Der HeggeZijnen [9]. He used this concept to explain the saddle-shape velocity profile formation. Experimental visualisation and detailed discussion of the role of coherent vortical structures, named “rolled-up azimuthal vortex structures”, in the switch-of-axes phenomenon for subsonic asymmetric jets was provided in studies [26], [27].
In 1994 Quinn [28] analysed detailed measurements of time averaged velocity profiles and turbulence characteristics for a plane nozzle air jet with AR=20 and nozzle velocity 60 m/s. He hypothesised that curvature variation of the rectangular azimuthal vortex will result in its non-uniform self-induction, which will generate secondary vortexes in a streamwise direction also contributing to the axis switching and jet shape change from rectangular to elliptic, and facilitating enhanced mixing of the jet. In 1996 Zaman [29] supported the point of view that not only azimuthal vortex, but also streamwise vortex pairs, generated in asymmetric jets, contribute to the switch-of-axes phenomenon and affect the mixing dynamics. The role of self-induced streamwise vorticity in axis switching and enhanced mixing of subsonic rectangular jets was confirmed using CFD technique in the numerical study by Wilson and Demuren in 1998 [30]. In the same year Elangovan and

Rathakrishnan [31] attributed the switch-of-axes phenomenon in sonic and supersonic (M=1.3) flows by the coherent vortical structures as well.

In 1998 Rajakuperan and Ramaswamy [23], studying under-expanded jets from oval nozzles with pressure ratios up to 20.3 and nozzle aspect ratio up to 5.0, concluded that the axis switching is caused by the complex interaction of expansion and compression waves. They didn't mention the role of azimuthal vortex structure in the axis switching.

It is worth noting that publications on the control of jets from elongated nozzles cover mostly subsonic jets. For example, the control of elliptic jets using sound excitation was studied in 1983-1989 by Husain and Hussain [27], [32]. They succeeded to switch axes of exited air jet not once but twice and to retain after that the two-dimensionality of the jet further downstream, where the "unexcited" jet already demonstrated close to axisymmetric jet behaviour [27].

In 1996 Zaman [29] demonstrated the use of in-nozzle tabs to control axis switching for subsonic plane air jets: tabs on the shorter nozzle walls lead to faster axis switching, while notches on the longer walls delayed switching. In 1998 Elangovan and Rathakrishnan [31] studied the effect of semi-circular cut-outs (notches) on air jet spread in fully expanded sonic and under-expanded jets (up to M=1.52) from a rectangular nozzle with AR=8.53. The under-expanded jet had the crossover distance closer to the nozzle compared to fully expanded jet. Slots with cut-outs on the minor axis (longer side) showed higher jet spread and faster velocity decay, according to authors - due to secondary vortices generated by cut-outs at the minor axis ends.

This overview demonstrated that there are controversial data on how plane jets decay compared to the round jets of the same size. Theory predicts slower decay of concentration in plane infinite (2D) jet compared to the round one. However, some experimental results obtained for plane jets with finite aspect ratio indicate that plane jet can decay faster. There is the lack of data on hydrogen jets from plane nozzles. Existing data on hydrogen are limited for reacting jets by pressure ratios up to 400, and plane nozzle aspect ratio up to 12.8. The behaviour of highly under-expanded unignited hydrogen plane nozzle jets is not predictable at the moment and experimental measurements are absent. This knowledge gap has to be closed, for instance, to provide background for engineering design of pressure relief devices (PRD) with reduced deterministic separation distances. This will be done in this study through undertaking numerical experiments using the CFD technique.

This paper aims to study numerically behaviour and structure of highly under-expanded hydrogen plane jets issued from round and plane nozzles of different aspect ratios, and understand the concentration decay downstream as far as 3,000 calibres (based on the diameter of round nozzle of the same cross-section area), where the hydrogen concentration in air drops below the lower flammability limit of 4% by volume.

2 Problem formulation

2.1 Modelling approach and the governing equations

The considered problem presents a disparity of spatial and velocity scales, precluding simulations of the flow in a single computational domain from inside the nozzle down to the end and beyond the flammable envelope location or the flame tip location. On one hand, a presence of the under-expanded jet shock structure associated with high flow velocities in a near field and a small aperture of the nozzle would dictate small time step for unsteady simulations. On the other hand, a large size of flammable envelope or jet flame and related hot current compared to the nozzle size, and slow velocities in the far from the nozzle field would require substantial computing resources and calculation of long real times. This makes simulation of the problem in one computational domain impractical.

To reduce the computational effort the problem was modelled in two stages: first the compressible flow in the near-to-nozzle field was simulated, then the results were used as boundary conditions for the far-from-nozzle field simulations where the incompressible flow approach is applied. The mathematical model includes three-dimensional Favre-averaged mass, momentum, energy and hydrogen conservation equations respectively as follows

$$\frac{\partial \bar{\rho}}{\partial t}+\frac{\partial}{\partial x_j}\left(\bar{\rho}\tilde{u}_j\right)=0, \tag{1}$$

$$\frac{\partial \bar{\rho}\tilde{u}_i}{\partial t}+\frac{\partial}{\partial x_j}\left(\bar{\rho}\tilde{u}_j\tilde{u}_i\right)=-\frac{\partial \bar{p}}{\partial x_i}+\frac{\partial}{\partial x_j}\left(\mu+\mu_t\right)\left(\frac{\partial \tilde{u}_i}{\partial x_j}+\frac{\partial \tilde{u}_j}{\partial x_i}-\frac{2}{3}\frac{\partial \tilde{u}_k}{\partial x_k}\delta_{ij}\right)+\bar{\rho}g_i, \tag{2}$$

$$\frac{\partial}{\partial t}\left(\bar{\rho}\tilde{E}\right)+\frac{\partial}{\partial x_j}\left(\tilde{u}_j\left(\bar{\rho}\tilde{E}+\bar{p}\right)\right)=$$

$$=\frac{\partial}{\partial x_j}\left(\left(k+\frac{\mu_t c_p}{Pr_t}\right)\frac{\partial \tilde{T}}{\partial x_j}-\sum_m \tilde{h}_m\left(-\left(\rho D+\frac{\mu_t}{Sc_t}\right)\frac{\partial \tilde{Y}_m}{\partial x_j}\right)+\tilde{u}_i\left(\mu+\mu_t\right)\left(\frac{\partial \tilde{u}_i}{\partial x_j}+\frac{\partial \tilde{u}_j}{\partial x_i}-\frac{2}{3}\frac{\partial \tilde{u}_k}{\partial x_k}\delta_{ij}\right)\right)+S_E, \tag{3}$$

$$\frac{\partial \bar{\rho}\tilde{Y}_{H_2}}{\partial t}+\frac{\partial}{\partial x_j}\left(\bar{\rho}\tilde{u}_j\tilde{Y}_{H_2}\right)=\frac{\partial}{\partial x_j}\left(\left(\rho D+\frac{\mu_t}{Sc_t}\right)\frac{\partial \tilde{Y}_{H_2}}{\partial x_j}\right)+S_{H_2}. \tag{4}$$

where x_i,x_j,x_k are Cartesian coordinates, u_i,u_j,u_k are velocity components, t is the time, p is the pressure, ρ is the density, g_i is gravity acceleration, μ_t is the turbulent dynamic viscosity, δ_{ij} is Kronecker symbol, E is the total energy, T is the temperature, Y_{H2} is the hydrogen mass fraction, c_p is the specific heat at constant pressure, Sc_t is the turbulent Schmidt number, Pr_t is the turbulent Prandtl number, D is the molecular diffusivity, m is the index of chemical specie (species are: H_2, O_2, H_2O, N_2), S_E is the source term in energy conservation equation due to combustion (when hydrogen jet flame is modelled), S_{H_2} is the source term in the hydrogen transport equation due to combustion. Symbol "overbar" stands for Reynolds averaged parameters and "tilde" for Favre averaged parameters.

Flow turbulence was modelled using standard k-ε turbulence model [33]

$$\frac{\partial\left(\bar{\rho}\bar{k}\right)}{\partial t}+\frac{\partial}{\partial x_j}\left(\bar{\rho}\tilde{u}_j\bar{k}\right)=\frac{\partial}{\partial x_j}\left(\left(\mu+\frac{\mu_t}{\sigma_k}\right)\frac{\partial \bar{k}}{\partial x_j}\right)+G_k+G_b-\bar{\rho}\bar{\varepsilon}, \tag{5}$$

$$\frac{\partial\left(\bar{\rho}\bar{\varepsilon}\right)}{\partial t}+\frac{\partial}{\partial x_j}\left(\bar{\rho}\tilde{u}_j\bar{\varepsilon}\right)=\frac{\partial}{\partial x_j}\left(\left(\mu+\frac{\mu_t}{\sigma_\varepsilon}\right)\frac{\partial \bar{\varepsilon}}{\partial x_j}\right)+C_{1\varepsilon}\frac{\bar{\varepsilon}}{\bar{k}}\left(G_k+C_{3\varepsilon}G_b\right)-C_{2\varepsilon}\bar{\rho}\frac{\bar{\varepsilon}^2}{k}, \tag{6}$$

where k is the turbulent kinetic energy, ε is the dissipation rate of turbulent kinetic energy, $\mu_t=\bar{\rho}c_m\bar{k}^2/\bar{\varepsilon}$, $G_b=-g_i\left(\mu_t/\bar{\rho}\,\mathrm{Pr}_t\right)\left(\partial\bar{\rho}/\partial x_i\right)$, c_m=0.09, σ_k=1.0, σ_e=1.3, $C_{1\varepsilon}$=1.44, $C_{2\,\varepsilon}$=1.92, $c_{3\varepsilon}=\tanh\left|\tilde{u}_y/\left(\tilde{u}_x^2+\tilde{u}_z^2\right)^{0.5}\right|$. Turbulent Schmidt and Prandtl numbers were equal $Sc_t=0.7$ and $\mathrm{Pr}_t=0.85$ respectively.

The Eddy Break-Up (EBU) combustion model [34] was employed for combustion modelling. The hydrogen source term (mass burning rate per unit volume) was modelled as

$$S_{H_2}=-C\bar{\rho}\frac{\bar{\varepsilon}}{\bar{k}}\min\left\{\tilde{Y}_{H_2},\frac{\tilde{Y}_{O_2}}{s}\right\}, \tag{7}$$

where C =4.0 is the empirical coefficient, $\tilde{Y}_{H_2}$ is the mass fraction of hydrogen, $\tilde{Y}_{O_2}$ is the mass fraction of oxygen, s=8.0 is the stoichiometric coefficient for hydrogen-oxygen reaction.

The EBU combustion model assumes that the reaction rate is infinitely fast and combustion is controlled by turbulent mixing only, hence unable, for example, to predict lift-off of turbulent flames. However, in this paper

we are focused on the prediction of axisymmetric and plane turbulent non-premixed flame length, and in first instance we neglect by insignificant effect of lift-off on the jet flame length. Indeed, the lift-off distance of hydrogen flames is not more than 0.08 m [35], and the length of experimental jet fires in [25] is in the range 1.0 – 2.6 m.

2.2 Calculation domain, boundary conditions and numerical details

The geometry simulated reproduces the details of the experiment [25]. Three nozzles were modelled: a round nozzle of 1.0 mm diameter and two plane nozzles having overall size 2.0 × 0.4 mm (length to width aspect ratio AR=5.0) and 3.2 × 0.25 mm (length to width aspect ratio AR=12.8), all three having the same cross section area.

Figure 1 shows computational domains and types of boundary conditions for compressible flow in the near-to-nozzle field and for incompressible flow in the far-from-nozzle field for the round nozzle jet. Calculation domain for the near-to-nozzle field had dimensions L (length)×D (diameter)=0.1625×0.104 m, the domain was discretised using 412,736 hexahedral control volumes (CVs). The round nozzle of 1 mm diameter was discretised using 20 CVs across the nozzle diameter. Domain for the far field had dimensions L×D=7.8×2.0 m and was discretised using 356,868 hexahedral CVs. Figure 1a shows the location of the interface from which solution of the compressible stage was passed to the incompressible stage as its boundary condition. The interface was located far from the compressible boundary to minimize potential effect of its numerical approximation errors onto the incompressible stage boundary conditions.

The calculation domains for the plane nozzle were designed similarly, apart from the fact that the domains utilized symmetry in the vertical plane (simulations were carried out for a half of the plane nozzle jet). Domain for the near field of AR=5.0 ratio nozzle had dimensions L×D=0.26×0.16 m. It was discretised by a hybrid mesh with a mix of tetrahedral and hexahedral CVs using in total 530,546 CVs, and the nozzle was discretised using 6 CVs across its width and 14 CVs across its half-length. A domain for the near field of AR=12.8 nozzle had the same dimensions, but its nozzle was discretised using 6 CVs across the width and 32 CVs across the half-length, total CV number was equal 504,040. Calculation domain for the far field of both plane nozzle jets was of the same dimension L×D=3.1×4.0 m and was discretised using 868,546 hexahedral CVs.

To improve stability and to avoid “flapping” of the simulated jets in the near-to-nozzle field, simulations were started as transient (unsteady) using explicit time marching, and switched to the steady-state simulations later on when the shock structure was established. Simulations in the far-field were run as steady-state thus neglected the transient term $\partial/\partial t$.

The standard k-ε turbulent model is known to overestimate the spread rate of axisymmetric jet as shown by Pope [36]. To avoid this effect the model was used here in conjunction with MUSCL third order approximation scheme following the study by Houf et al. [37], where reasonable velocity decay was achieved in simulations of a free incompressible axisymmetric hydrogen-air jet. Another approach could be a modification of the k-ε model coefficient, as it was applied by Galassi et al. in simulations of hydrogen tank filling in [38] following the study by Ouellette and Hill [39].

Numerical grids used for compressible and incompressible simulation stages were not identical at the outflow-inflow interface. An interpolation of simulation results was required at the inflow boundary of the incompressible stage domain. This potentially may deteriorate the accuracy of calculation results. Special attention was paid that key flow parameters at the interface between compressible and incompressible domains were matching each other. Table 1 gives relative errors for the hydrogen mass flow rate, the total impulse, the maximum hydrogen mass fraction and the maximum absolute velocity at the compressible outflow/incompressible inflow interface between the domains for all three simulated cases. The error is relatively small and a smooth, continues solution through both domains was preserved.

Table 1 shows that the total hydrogen mass flow rate through the whole nozzle geometry (keeping in mind that only half of a jet was simulated in case of AR=5.0 and AR=12.8 nozzles using the symmetry condition). Values are comparable and close to each other, i.e. 1.56, 1.52 and 1.36 g/s of hydrogen for the round, AR=5.0, and AR=12.8 nozzles respectively. The difference of 15% can be explained by the increase of losses in the flow pathway with a minimum of losses for the round nozzle and then the increase of losses for plane nozzles with the increase of the aspect ratio.
The simulations were carried out using the software ANSYS Fluent 13. The density-based explicit solver was applied for solving compressible part of the problem, and the pressure-based implicit solver was used for incompressible simulations.

3 Non-reacting hydrogen jet simulation results

3.1 Hydrogen flammable envelope and axial concentration decay

Figure 2 shows hydrogen concentrations in a range 4-100% vol. in the cross section parallel to the principal jet axis and in a number of selected cross sections perpendicular to the axis for non-reacting jets from the round nozzle (a), and plane nozzles with AR=5 (b) and 12.8 (c). The major axis of both plane nozzles is oriented horizontally. Simulation results are visualised here for the far-from-nozzle field, hence sharp hydrogen distribution cut-off is seen on the left hand side in Fig. 2 where hydrogen enters the domain through the inflow boundary, i.e. the interface with the close-to-nozzle domain. The longest flammable envelope, i.e. distance to the lower flammability limit (LFL) of 4% by volume of hydrogen in air, is observed for simulated axisymmetric jet from the round nozzle. The flammable envelope of the round nozzle jet propagates as far as 4.1 m downflow. The jet is in the momentum-dominated regime at least up to LFL and its normal to the axis cross-section profiles retain round shape.

Flammable envelope for both plane nozzles is flattened in the vertical plane, i.e. it has larger size in vertical direction along the minor axis and smaller size in horizontal direction along the major axis. Apparently, simulated under-expanded plane nozzle jets have higher spread rate in the vertical direction (see Fig. 2). This is in full agreement with the switch-of-axes phenomenon that will be analysed in more detail in the next section. The flattened hydrogen jet naturally has larger “mixing layer” area compared to the axisymmetric jet. This results in a more intensive mixing with ambient air and leads to a shorter flammable envelope.

The distance to LFL for the plane nozzle with AR=5.0 is only 2.8 m downflow, i.e. 1.5 times shorter compared to the round jet, and plane jet with AR=12.8 is even shorter - 2.25 m, i.e. 1.8 times shorter than the axisymmetric jet of the same cross-section area. This is an essential reduction of the separation distance with practically the same mass flow rate, which is slightly affected by friction losses in the leak pathway.

Figure 3 shows hydrogen mass fraction versus distance at the centreline for the axisymmetric jet, and both at the centreline and distance to the maximum concentration (“saddle-shape” profile) for the plane nozzle jets. The similarity law for axial concentration decay in axisymmetric jets [8], validated recently for under-expanded jets [40], is shown in Fig. 3 for comparison too

$$y_{H2} = 5.4\left(D/x\right)\left(\rho_N/\rho_S\right)^{0.5}. \quad (8)$$

All data is presented as a function of a non-dimensional coordinate $\bar{x} = x/5.4D\left(\rho_N/\rho_S\right)^{0.5}$, so that the similarity law for axisymmetric jet (8) takes the form $y_{H2} = 1/\bar{x}$. Figure 3 shows also the horizontal line corresponding to 4% by volume of hydrogen (LFL) and the dashed line representing the similarity law for concentration decay in infinite 2D jets [8]

$$y_{H2} = 2.13\left(D/x\right)^{0.5}\left(\rho_N/\rho_S\right)^{0.5}, \quad (9)$$

where D is the plane nozzle width. Being presented as a function of the same non-dimensional coordinate $\overline{x}$, the 2D similarity correlation takes the form $y_{H2} = 2.13/(5.4)^{0.5}\left(\rho_N/\rho_S\right)^{0.25}\left(1/\overline{x}\right)^{0.5}$. Hydrogen density at the nozzle exit at storage pressure 40MPa was calculated as ρ_N=16.23 kg/m^3, using the under-expanded jet theory [41]. It should be noted that hydrogen densities obtained in CFD simulations at the nozzle exit are affected by friction losses along the nozzle walls, but remain close to the analytically calculated value: density in the cross-section of the round nozzle varied in the limits ρ_N=15.4-17.2 kg/m^3, density in the nozzle with AR=5 - ρ_N=16.2-17.5 kg/m^3, density in the nozzle with AR=12.8 - ρ_N=15.7-17.6 kg/m^3. Taking into account that the density ratio in the similarity laws (8) and (9) is under the square root, the use of the analytically calculated density in correlations (8) and (9) may lead to the maximum error of ±4% compared to densities obtained in CFD simulations. Density of ambient air is taken as ρ_S=1.20 kg/m^3.

It should be noted that originally both correlations of Chen and Rodi [8] were developed for incompressible expanded jets and are applicable at some distance from the nozzle. The simulations showed that the onset of the incompressible flow regime ($M \le 0.33$) is at $x \approx 0.25$ m for the round nozzle jet, $x \approx 0.12$ m for the AR=5 plane nozzle jet, and $x \approx 0.10$ for the AR=12.8 plane nozzle jet. This is in the dimensionless coordinates $\overline{x} \approx$ 12.6, 6.0 and 5.0 respectively (equal cross-section area diameter D=1 mm was used for plane nozzles to find $\overline{x}$). In authors' previous experience the error introduced by initially compressible flow ($0.33 < M < 1$) into the incompressible downstream flow parameters is negligible, yet allows to speed up the simulations significantly. It is interesting to note that the static gauge pressure at inflow boundary of incompressible domain for all three studied cases changes within limits -410 to +720 Pa, which may lead to the calculation error in jet density of ±0.7% only, i.e. the effect of compressibility can be neglected.

The comparison of correlations (8) and (9) in Fig. 3 shows that the concentration decay due to air entrainment in the ideal infinitely long 2D jet (AR=∞) should be less intensive than in the axisymmetric jet. This is due to the smaller mixing area per unit mass rate of the jetted gas. However, simulations demonstrate that finite aspect ratio plane nozzle jets, on the contrary, are characterised by significantly faster concentration decay rate than the round nozzle jet and the similarity law for axisymmetric jets. This may be observed already at the initial stage of jet development, which may be seen from their faster concentration decay rate at dimensionless distances $\overline{x} \approx 1-3$ (see left part of Fig. 3), with the lowest concentration for the plane nozzle with highest simulated AR=12.8. This behaviour may be explained by a wider flattened hydrogen distribution profile developing in the course of the switch-of-axes phenomenon that provides larger mixing area per unit mass flow rate compared to the jet from the equivalent area round nozzle.

The axisymmetric jet core does not mix with ambient air before it passes Mach disk that is located at $\overline{x} = 0.6$ in our simulations, and decelerates to near sonic speeds, see next section for details. This offset between hydrogen concentration in the round and plane jets due to slow mixing of the round jet at the initial stage of its development mostly preserved further downstream in a well-developed region $\overline{x} > 30-40$.

Experimental evidence [10],[11],[27],[29] suggests that in the far field a plane nozzle jet development should be similar to an axisymmetric jet. In our simulations the focus is on the flammable envelope and the calculation domain was limited by this reason to include the area where hydrogen axial concentration decays to 4% by volume. This similarity was not achieved due to this restriction of the calculation domain and the plane nozzle jet remained flattened for the highly under-expanded jets studied. The result is similar to that in [15], where the jet profile retained plane-like shape, but centreline velocity decay yet was similar to that in axisymmetric jet.

Difference between maximum and centreline concentrations for AR=5.0 is up to 3% at $\overline{x} = 60$, but mostly negligible. Difference between maximum and centreline concentrations for AR=12.8 reaches 24% at $\overline{x} = 20$,

and decreases to around 20% with the growth of distance from the nozzle. The difference is due to the saddle-shape of velocity and concentration distribution (see Fig. 2).

Figure 3 demonstrates that hydrogen concentration decay in the round nozzle jet is faster than the decay rate predicted by the similarity law for axisymmetric jets even at far downstream locations. To exclude numerical error as a potential reason for this discrepancy an additional simulation was performed at incompressible stage with a finer numerical mesh to check the grid convergence. The total CVs number was 1,066,524, i.e. approximately 1.5 times finer CV size in all directions. Figure 4 shows that centreline concentration decay rates obtained for round nozzle jet using both coarser (356,868 CVs) and finer grids are identical.

Another additional simulation with a value of the k-ε turbulence constant $C_{\varepsilon 1} = 1.52$ instead of the standard value $C_{\varepsilon 1} = 1.44$ was carried out following conclusions by Ouellette and Hill [39] to study if the turbulence model could cause excessive diffusivity when applied to axisymmetric jets. Figure 4 shows that value of hydrogen concentration with $C_{\varepsilon 1} = 1.52$ is larger compare to the standard value $C_{\varepsilon 1} = 1.44$. However, the lines for centreline hydrogen concentration distribution with both coefficients are parallel and the concentration decay rate is exactly the same.

3.2 Axis switching phenomena and jet structure in near-to-nozzle field

Structures of plane and axisymmetric jets are examined in this section in order to understand the mechanism behind the switch-of-axes phenomenon.

The round nozzle under-expanded jet structure is well studied and its description may be found elsewhere, e.g. in fluid dynamics monograph [42]. Figure 5a shows a scheme of an axisymmetric under-expanded jet flow and a shock wave structure. For diatomic gases when nozzle exit to atmosphere pressure ratio reaches 1.89 the flow becomes choked, i.e. sonic velocity is reached and will not grow with further increase of the pressure ratio. It should be noted that the increase of mass flow rate with further increase of the pressure ratio is due to an increase in density. The under-expanded flow, i.e. pressure at the nozzle exit is above atmospheric, expands through a series of expansion waves when gas exits the nozzle. This is accompanied by gas acceleration to velocities above the local speed of sound (Mach number above 1.0) with corresponding decrease of pressure and density. The expansion diverges peripheral streamlines from their initial direction outward from the flow centreline. This defines larger flow boundary diameter compare to the actual nozzle diameter. At the flow boundary the expansion waves are reflected as compression waves. These waves form a supersonic compression flow and merge into an oblique (barrel) shock. The compression causes flow streamlines to turn back inwards. Closer to the jet centre the oblique shocks merge to form a direct shock called Mach disk. Upstream from Mach disk pressure is lower than ambient and flow is supersonic, behind Mach disk pressure grows up and flow becomes subsonic again. Yet, the streamlines peripheral to the Mach disk form supersonic flow which crosses oblique and reflected shocks (see Figure 5a). More than 90% of the total mass flow passes through this supersonic flow peripheral to Mach disk [43]. When nozzle to ambient pressure ratio is large ($n >> 1$) the losses in the direct shock preclude formation of next barrel shock, the flow acceleration is impossible and velocity remains subsonic [42].

Schlieren images of the under-expanded jet shock structure from an oval nozzle with AR=5 and pressure ratio n=20.3, from experimental study by Gutmark et al. [22], are shown in Fig. 5b. The shock structure of plane jet in its major axis resembled that of the axisymmetric jet: oblique shock, reflected shock and the direct shock corresponding to Mach disk are clearly seen. In the minor plane the barrel shock is generally absent, though the reflected shock and the “analogy” to the direct shock are present.

The structures of the round under-expanded jet and plane jet with AR=12.8 in near-to-nozzle area simulated in this study are presented in Fig. 6. Figure 6 is the overlap of numerical Schlieren images (density gradients) with the flow streamlines. Streamlines of entrained air into the jet are shown in blue and hydrogen streamlines are in red. In spite of using the first order upwind scheme, known to have larger numerical diffusion, to exclude

"numerical oscillation" the structure of the axisymmetric jet is reproduced well: barrel and reflected shocks, slip lines between subsonic and supersonic regions as well as flow boundary are seen. Slip lines are seen as thin sharp lines. Mach disk is blurred but distinguished. This is probably affected by elongated along the flow axis cells in this location. The reflected shock is indicated by the wide slightly darker area. The barrel shock is not penetrated by the entrained air streamlines in full agreement with the theory, and the space inside the barrel shock is filled with hydrogen only. There is an entrainment of air to the flow outside the barrel shock. A dark area around the barrel shock is seen due to large density gradient between air, hydrogen in the mainstream flow outside the barrel shock, and hydrogen within the barrel shock. Momentum exchange and mixing takes place in darker areas that can be seen from a sudden change of air streamlines direction. At the initial stage of jet development the angle of jet spread from this Schlieren image is about 10^0, but generally an under-expanded jet boundaries are curvilinear [42].

The same composite image for the plane AR=12.8 nozzle jet shows quite different shock and flow structure. Similar to experimental observation by Rajakuperan and Ramaswamy 23 shown in Fig. 5a the flow from the plane nozzle AR=12.8 (see Fig. 6, centre and right images) diverges with high spread rate in the minor axis plane (jet spread angle is about 77^0), converges in the major axis plane up to some distance, and then starts to diverge again (jet spread angle is about 6.5^0). This is a clear manifestation of the switch-of-axes phenomenon. The onset of axis switching is observed immediately at the nozzle exit, not at some crossover distance as observed in previous experimental studies at much lower storage pressures. The oblique shock may be seen in the simulated shock structure, but contrary to results of 23 (Fig. 5b) the Mach disk is totally degenerated, probably due to significantly larger pressure compared to that used in 23 and causing a larger spread rate. This is implicitly supported by the observation 21 that "the larger spread at the minor axis ... weakens the shock cell structure". The vertical element of shock structure, formed by merging oblique shocks and visible in minor axis, is located at distance x=0.008 m ($\overline{x} = 0.4$) from the plane nozzle, which is close to location of Mach disk from the circular nozzle - x=0.012 m ($\overline{x} = 0.6$). This implicitly supports experimental observations by Gannochenko et al. [19] who found that location of CCS for plane and axisymmetric jets at large pressure ratios $n>p_N/p_S$ practically coincides. The jet shape converging in major axis results in thin, flattened jet profile having much larger mixing area compare to the axisymmetric jet of the same characteristic size. This in turn affords more effective air entrainment and decreases hydrogen concentration already in the near-to-nozzle area.

Figure 7 shows cross-sections of the same round and plane AR=12.8 nozzle jets coloured by the value of mass flow rate per unit area. The largest mass flow rate in the axisymmetric jet passes through the peripheral zone outside the barrel shock. This is in full agreement with the theory, The plane nozzle jet provides more intensive mixing already in the near-to-nozzle area: the mass flow rate per unit flow area for the plane nozzle jet quickly falls down to 150-200 kg/s/m^2 at x=0.04 m, while the same for the axisymmetric jet is maintained at 250-300 kg/s/m^2 far beyond x=0.04 m mark, thus transporting nearly undiluted hydrogen downflow. Larger mass flow rate located far off centre-line in the minor plane could explain the formation of the saddle shape structure of the jet (two sharp picks in mass flow rate close to the main axis are probably due to numerical issues with the use of the symmetry plane in simulations to reduce CPU time).

Figure 8 shows distribution of Mach number (cut-out at M=1.0) both in the jets centreline cross-sections, and four cross-sections perpendicular to the centreline at different distances from the nozzle. The plane jet is "slower" than the axisymmetric jet already in the vicinity to nozzle, i.e. the maximum Mach number for the axisymmetric jet reaches M=8 at some distance from the nozzle close to Mach disk, while the maximum Mach number for the plane nozzle jet is only M=5. Mach number profile for the plane nozzle jet shows that there is no crossover distance and the jet width in the direction of minor axis is larger than the jet width in the direction of major axis already at the nozzle exit. At distance x=5 mm the ratio of jet width in the minor axis plane to that in the major axis plane is already about 3. Further downstream the vertical size of the plane jet continues to grow leading to the formation of a tall and a thin jet profiles. Small flow structures developing at the centre of the jet parallel to the major nozzle axis were obtained for the nozzle with AR=5 as well and are similar to those obtained in simulations by Usami et al. [24] for their nozzle with AR=8 and pressure ratio 50.

Figure 9 shows the combined images of pressure and pressure gradient distributions in the minor (a) and the major (b) axis cross-sections of the plane AR=12.8 nozzle jet. Black-and-white parts of both snapshots (below the symmetry plane) are presenting the overpressure above atmospheric level. The colour parts of snapshots represent pressure gradients for the minor ($\partial p/\partial y$) and the major ($\partial p/\partial z$) axis respectively. The pressure gradients $\partial p/\partial y$ and $\partial p/\partial z$ may be interpreted as "volumetric forces" in the momentum conservation equations (2) along OY and OZ axes forcing gas to change the flow velocity direction. Though maximum pressure gradient reaches value $8{\cdot}10^{10}$ Pa/m, the colour map is scaled only up to $2{\cdot}10^{9}$ Pa/m to better visualise the pressure gradient distribution around nozzles.

Figure 9a demonstrates that the whole flow passing through the nozzle is affected by the pressure gradient in the direction of the minor axis $\partial p/\partial y$ and hence is the subject to the upward force. Figure 9b shows the pressure gradient $\partial p/\partial z$ .The force in the major axis direction is applied to only the part of the flow in the vicinity of nozzle edges, and along the minor axis to the whole flow. This is the major reason for the switch-of-axes phenomenon in the under-expanded plane nozzle jets. The axis switching occurs immediately at the nozzle exit that excludes the influence of viscous forces on the switch-of-axes phenomenon in highly under-expanded flows.

3.3 Effect of pressure on axis switching

Figure 10 shows simulated distribution of hydrogen mass fraction in the major and minor axis planes obtained for the plane nozzle AR=12.8 at different hydrogen storage pressure of 0.5, 2, 10 and 40 MPa respectively. The pressure has direct impact on the axis switching: the higher pressure, the more pronounced the jet spread rate in the minor axis plane. This in line with the suggestion made by Krothapalli et al. [15] that higher pressure ratios should preserve the two-dimensionality of a jet further downstream.

At storage pressure 0.5 MPa the jet width in the minor axis plane is comparable with that in the major axis plane and there is no "strong" switch of axes in this case and the jet cross-section profile at the exit from calculation domain is rather axisymmetric. However, at pressure 2 MPa the axis switching is clearly distinguishable and very close to the nozzle: immediately on exit from the nozzle the jet width in the major axis plane slightly shrinks, while in the minor axis plane the spread rate is essentially higher compared to the case with 0.5 MPa storage pressures. At pressure 10 MPa the growth rate of the jet width in the minor axis plane is even higher and monotonic. There is still significant shrinking of the hydrogen flow in the major axis direction. At the highest storage pressure of 40 MPa the hydrogen spread angle doesn't change noticeably to pressure 10 MPa case, but the hydrogen concentration distribution is more uniform across the field.

4 Validation of a CFD model against hydrogen jet fire experiment

The described above CFD EBU model [34] was applied to simulate experiments by Mogi and Horiguchi of jet fires from round and plane nozzles studied above for unignited jets [25]. Figure 11 gives the side view of the experimental jet fire in comparison with the axial cross-section of the simulated jet fire. The simulated jet fire was visualised using temperature profile in the range T=1300-2300 K, similar to [44]. The simulated jet fire shape and length are reproducing well the experimental data. Both experiments and simulations demonstrate that the plane nozzle jet fire is wider yet shorter than the axisymmetric jet fire from the round nozzle of the same cross-section area. The experimental round nozzle jet fire length is reported as about 2.6 m and the plane nozzle jet fire is more than 2 times shorter – only 1.1 m [25]. Experimental photographic images show somewhat shorter "visible" flames. This is probably due to a limited colour reproduction in a typographical process as well as difficulties in the visualisation of hydrogen flames.

Figure 12 shows the front view of the same experimental jets in comparison with the front view of the simulated iso-surface of temperature T=1300 K. The simulated round nozzle jet is not perfectly axisymmetric and exhibits

to some degree the buoyancy effect. Yet, this is far from the vertically oriented close-to-plane appearance of the jet fire from the horizontally oriented plane nozzle, which is similar to the respective experimental image.

These simulations demonstrate that the impact of physical and numerical features, which potentially could deteriorate results, is acceptable. Use of standard k-ε model with MUSCL approximation scheme, compressible/incompressible two stage modelling, incompressible formulation for the second stage inflow boundary, perfect gas law for hydrogen at 40 MPa does not lead to appreciable error in the predictive capability of the model. The CFD model was using the equation of state for perfect gas. The mass flow rate through the round 1 mm nozzle calculated by the perfect gas law in the absence of losses is 19.58 g/s, while using the Abel-Noble real gas equation of state it is 16.87 g/s. This 16% difference shouldn't have a profound effect on the simulation results.

Mogi and Horiguchi [25] didn't report the mass flow rate for each of the jets, making it difficult to judge if the shorter jet flame length was a result of the smaller mass flow rate due to pressure losses in the narrower plane nozzles. The simulation results show only 15% difference in mass flow rate (see Table 1), which makes effect of pressure losses negligible compare to such a dramatic decrease of the flame length.

5 Conclusions

Simulations of non-reacting under-expanded hydrogen jets from three nozzles having the same cross-sectional area are carried out to study the difference in structure and parameters of the jets in the near and far from the nozzle field. The flammable envelope shape is analysed for 1 mm diameter round nozzle and two plane nozzles with aspect ratio 5.0 and 12.8 respectively.

CFD simulations were performed by the two-stage technique. The compressible solver was applied to simulate shock structure and supersonic hydrogen flow in the near to the nozzle field, and the incompressible flow solver was used for simulations in far from nozzle field. This modelling approach was validated against experiments by Mogi and Horiguchi (2009) on hydrogen jet flames from the same nozzles as in the study of unignited jets.
The longest flammable envelope is simulated for the round nozzle jet and reached about 4.2 m. The plane nozzle jets produced shorter flammable envelopes, i.e. 2.8 m and 2.3 m for nozzles with aspect ratios 5.0 and 12.8 respectively. Simulated concentrations in the far field of the round nozzle jet were somewhat lower compared to the similarity law for under-expanded axisymmetric jets. However, the concentration decay rate was slightly faster than predicted by the similarity law. The hydrogen concentration decay rate of the plane nozzle jets was close to the similarity law for an axisymmetric jet rather than for an infinite 2D plane jet.

The switch-of-axes phenomenon was reproduced in simulations for both reacting and non-reacting hydrogen jets. It was demonstrated for the first time that at storage pressures as high as few tens of MPa there is no crossover distance for the onset of the axis switching. The process of axis switching takes place right at the nozzle exit. It is concluded based on the performed analysis of simulation results that the immediate switch-of-axes for highly under-expanded jets is caused by larger area of pressure gradients in the minor axis direction compared to the major axis direction. The jet expands with higher spread rate in the minor axis direction leading to the switch-of-axes phenomena. The plane jet formed in this way has flattened profile that is perpendicular to the major axis of plane nozzle.

The results can be applied in hydrogen safety engineering, e.g. to design release from the pressure relief devices that have to be installed at all on-board storage tanks of hydrogen-powered vehicles.

6 References

[1]. Wakes SJ, Holdo AE, Meares AJ. Experimental investigation of the effect orifice shape and fluid pressure has on high aspect ratio cross-sectional jet behaviour. Journal of Hazardous Materials 2002; A89:1-27.
[2]. Schlihting H. LaminareStrahlausebreitung. ZAMM 1933; 13:260-3.

[3]. Bickley WG. The plane jet. Phil. Mag. S.7 1937; 23:156:727-31.
[4]. Schlihting H. Boundary-Layer Theory. McGraw-Hill:New-York; 1979.
[5]. Vulis LA, Terekhina NN. J. Tech. Phys. 1955; 26:1249-63.
[6]. Ricou FP, Spalding DB. Measurements of entrainment by axisymmetric turbulent jets, Journal of Fluid mechanics 1961; 8:21-32.
[7]. Abramovich GN. The theory of turbulent jets. M.I.T. press:Cambridge, Mass; 1963.
[8]. Chen CJ, Rodi W. Vertical turbulent buoyant jets – review of experimental data. In: Spalding DB, Editor-in-chief. The Science and applications of heat and mass transfer. Vol.4. Pergamon Press;1980.
[9]. Van Der HeggeZijnen BG. Measurements of the velocity distribution in a plane turbulent jet of air, Appl. Sci. Res. Section A 1957; 7:256-92.
[10]. Sforza PM, Steiger MH, Trentacoste N. Studies on three-dimensional viscous jets, AIAA J. 1966; 4:5:800-6.
[11]. Trentacoste N, Sforza P. Further experimental results for three-dimensional free jets, AIAA J. 1967; 5:5: 885-91.
[12]. Sfeir AA. Investigation of three-dimensional turbulent rectangular jets, AIAA journal 1979; 17:10:1055-60.
[13]. Krothapalli A, Baganoff D, Karamcheti K. On the mixing of a rectangular jet, J. Fluid Mechanics 1981; 107:201-20.
[14]. Hsia Y, Krothapalli A, Baganoff D, Karamcheti K. The structure of a subsonic compressible rectangular jet. NASA-CR-169110; SU-JIAA-TR-43 (Jan 1, 1982) 1982.
[15]. Krothapalli A, Hsia Y, Baganoff D, Karamcheti K. On the structure of an underexpanded rectangular jet. NASA-CR-169734; SU-JIAA-TR-47 (Jul 1, 1982) 1982.
[16]. Schadow KC, Wilson KJ, Lee MJ, Gutmark E. Enhancement of mixing in reacting fuel-rich plumes issued from elliptical nozzles, Journal of Propulsion and Power 1987; 3:2:145-9.
[17]. Crane LJ, Pack DC. The laminar and turbulent mixing of jets of compressible fluid. Part I Flow far from the orifice, Journal of Fluid Mechanics 1957; 2:5:449-55.
[18]. Maydew RC, Reed JF. Turbulent mixing of compressible axisymmetric jets (in the half region) with quiescent air, Sandia Corp. Res. Rept SC-4764 (March 1963) 1963.
[19]. Gannochenko GI, Ermolayev LS, Zadorozhnyi NA. On the position of the central compression shock in underexpanded sonic jet issuing from a slot nozzle, J. Appl. Mech. Tech. Physics 1986; 27:4:559-61.
[20]. Schadow KC, Gutmark E, Koshigoe S, Wilson KJ. Combustion-related shear-flow dynamics in elliptic supersonic jets, AIAA Journal 1989; 27:10:1347-53.
[21]. Gutmark E, Schadow KC, Wilson KJ. Noncircular jet dynamics in supersonic combustion. Journal of Propulsion and Power 1989;5:5:529-33.
[22]. Gutmark E, Schadow KC, Bicker CJ. Near acoustic field and shock structure of rectangular supersonic jets. AIAA Journal 1990; 28:7:1163-70.
[23]. Rajakuperan E, Ramaswamy MA. An experimental investigation of underexpanded jets from oval sonic nozzles. Experiments in Fluids 1998; 24:4:291-9.
[24]. Usami M, Niimi S, Imura T, Takahashi T. DSMC calculation of supersonic free jet through a rectangular or a multi-aperture orifice by an improved new collision scheme. Proc. 26th International Symposium "Rarefied Gas Dynamic". The Institution of Engineering and Technology 2008 (ISBN 0094-243X); 1135-40.
[25]. Mogi T, Horiguchi S. Experimental study on the hazards of high pressure hydrogen jet diffusion flame, Journal of Loss Prevention in the Process Industries 2009; 22:45-51.
[26]. Ho C-M, Gutmark E. Vortex induction and mass entrainment in a small-aspect-ratio elliptic jet. Journal of Fluid Mechanics 1987; 179:383-405.
[27]. Hussain F, Husain HS. Elliptic jets. 1. Characteristics of unexcited and excited jets. Journal of Fluid Mechanics 1989; 208:257-320.
[28]. Quinn WR. Development of a large aspect-ratio-rectangular turbulent free jet. AIAA Journal 1994; 32:3:547-54.

[29]. Zaman KBMQ. Axis switching and spreading of axisymmetric jet: the role of coherent structure dynamics, Journal of Fluid Mechanics 1996; 316:1-27.
[30]. Wilson RV, Demuren AO. Numerical simulation of turbulent jets with rectangular cross-section, Journal of Fluids Engineering, Transactions of the ASME 1998; 120:2:285-90.
[31]. Elangovan S, Rathakrishnan E. Effect of cut-outs on underexpanded rectangular jets, Aeronautical Journal 1998; 102:1015:267-75.
[32]. Husain HS, HussainAKMF. Controlled excitation of elliptic jets, Phys. Fluids 1983; 26:10:2763-6.
[33]. Launder BE, Spalding DB. The numerical computation of turbulent flow, Computational Methods in Applied Mechanical Engineering 1974; 3:269-89.
[34]. Magnussen BF, Hjertager BH. On mathematical modelling of turbulent combustion with special emphasis on soot formation and combustion. In Proceedings of Sixteenth Symposium (Int.) on Combustion. The Combustion Institute, Pittsburgh, PA;1976, p.719-729.
[35]. Mogi T, Nishida H, Shiina H, Horiguchi S. A study of combustion properties of high-pressure hydrogen gas jet. In Proceedings of 43rd Symposium (Japanese) on Combustion, 5-7 December 2005, Tokyo, Japan, pp.164-165.
[36]. Pope SB. An Explanation of the Turbulent Round-Jet/Plane-Jet Abnormality, Technical Note, AIAA J. 1978; 16:3:279.
[37]. Houf WG, Evans GH, Schefer RW. Analysis of jet flames and unignited jets from unintended releases of hydrogen, in Proceedings of 2nd International Conference on Hydrogen Safety, 11-13 September 2007, Paper ID 1.1.65, San-Sebastian, Spain.
[38]. Galassi MC., Papanikolaou E, Heitsch M, Baraldi D. Validation of CFD models for hydrogen fast filling simulations, Paper 166 in Proceedings of 4th ICHS, San-Francisco, USA, 12-14 September 2011.
[39]. Ouellette P, Hill PG. Turbulent Transient Gas Injections, Journal of Fluids Engineering 2000; 122:743–53.
[40]. Molkov V. Fundamentals of hydrogen safety engineering. Proceedings of the 4th European Summer School on Hydrogen Safety, 7-16 September 2009, Corsica, France.
[41]. Molkov V, Makarov D, Bragin M. Physics and modelling of under-expanded jets and hydrogen dispersion in atmosphere, in Fortov V.E., et al. (eds) Physics of extreme state of matter 2009.Chernogolovka, Russia, pp. 143-145, 2009, ISBN 978-5-901675-89-2.
[42]. Abramovich GN. Applied gas dynamics. Third Ed., Defence Technical Information Center; 1973.
[43]. Chizhikov AS. On the gas flow rate through a Mach disk in an underexpanded jet, Journal of Engineering Physics and Thermophysics 2009; 82:315-20.
[44]. Brennan SL, Makarov DV, Molkov V. LES of high pressure hydrogen jet fire, Journal of Loss Prevention in the Process Industries 2009: 22:3:353-9.

Figure captions

Figure 1. Computational domains: a) domain for the near-to-nozzle field (round nozzle), b) domain for the far-from-nozzle field (round nozzle), c) round nozzle mesh, d) AR=5.0 nozzle mesh, e) AR=12.8 nozzle mesh.

Figure 2. Hydrogen volume fraction distribution in the range $X(H_2)$=0.04-0.75 in the jet cross-section (along the minor axis for plane nozzles): a) round nozzle, b) plane nozzle AR=5.0, c) plane nozzle AR=12.8.

Figure 3. Simulated hydrogen mass fraction decay in comparison with the similarity law for under-expanded jets [41] (equivalent nozzle diameter D_{eq}=1 mm, hydrogen density in the nozzle ρ_N=16.23 kg/m^3 (40 MPa), ambient air density at NTP ρ_S=1.20 kg/m^3).

Figure 4. The effects of grid resolution and modified $C_{\varepsilon 1}$ coefficient in the k-ε turbulence model on the centreline concentration decay in the axisymmetric jet.

Figure 5. Under-expanded jet shock structure: a) round nozzle jet, b) oval nozzle jet AR=5 23.

Figure 6. Schlieren images and streamlines for simulated axisymmetric (left) and plane (centre and right) nozzle jets (blue – streamlines of entrained air, red – hydrogen).

Figure 7. Distribution of mass flow rate for the axisymmetric jet and the plane nozzle jet with AR=12.8.

Figure 8. Mach number distribution for the axisymmetric and the plane AR=12.8 nozzles: a) centreline cross-section; and cross sections at: b) x=0.0 m, c) x=0.005 m, d) x=0.010 m, e) x=0.015 m.

Figure 9. a) Pressure and pressure gradient $\partial p/\partial y$ in the minor axis cross-section, b) pressure and pressure gradient $\partial p/\partial z$ in the major axis cross-section.

Figure 10. Effect of storage pressure on the axis switching for the plane nozzle AR=12.8 (left – the minor axis cross-section, right – the major axis cross-section): a) 0.5 MPa, b) 2 MPa, c) 10 MPa, d) 40 MPa.

Figure 11. The side view of experimental jet flames [25] and simulated jet flame (temperature profiles in the range T=1300-2500 K): a) round nozzle, b) plane nozzle AR=12.8.

Figure 12. The front view of experimental jet flames [25] and simulated jet flame iso-surface of temperature T=1300 K: a) round nozzle, b) plane nozzle AR=12.8.

Figures

Figure 1

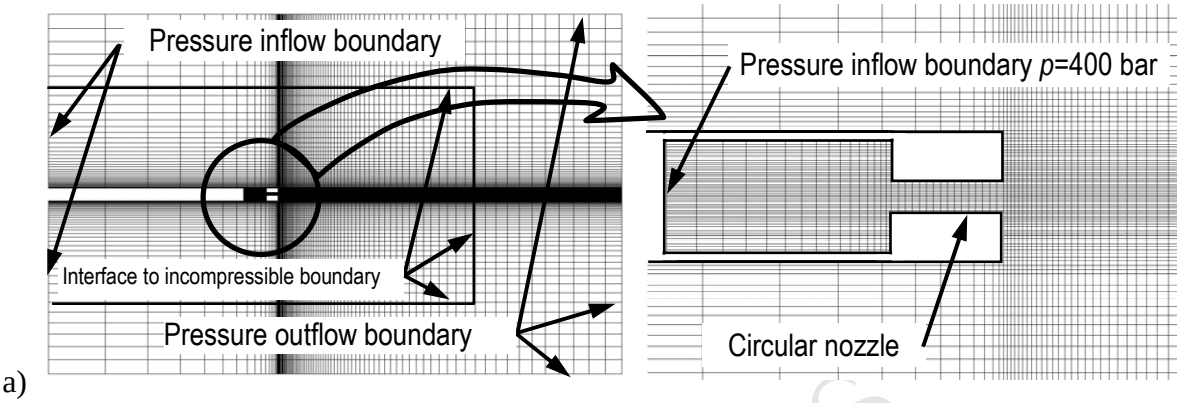

a)

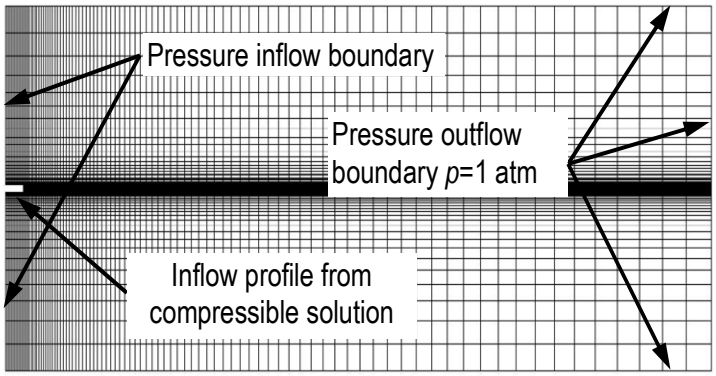

b)

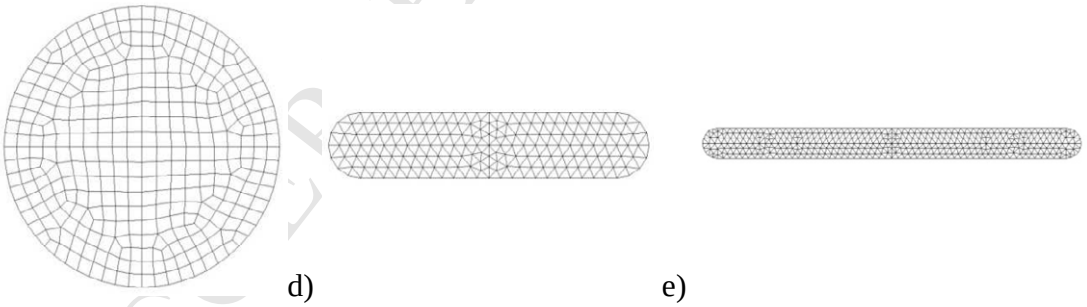

c) d) e)

Figure 2

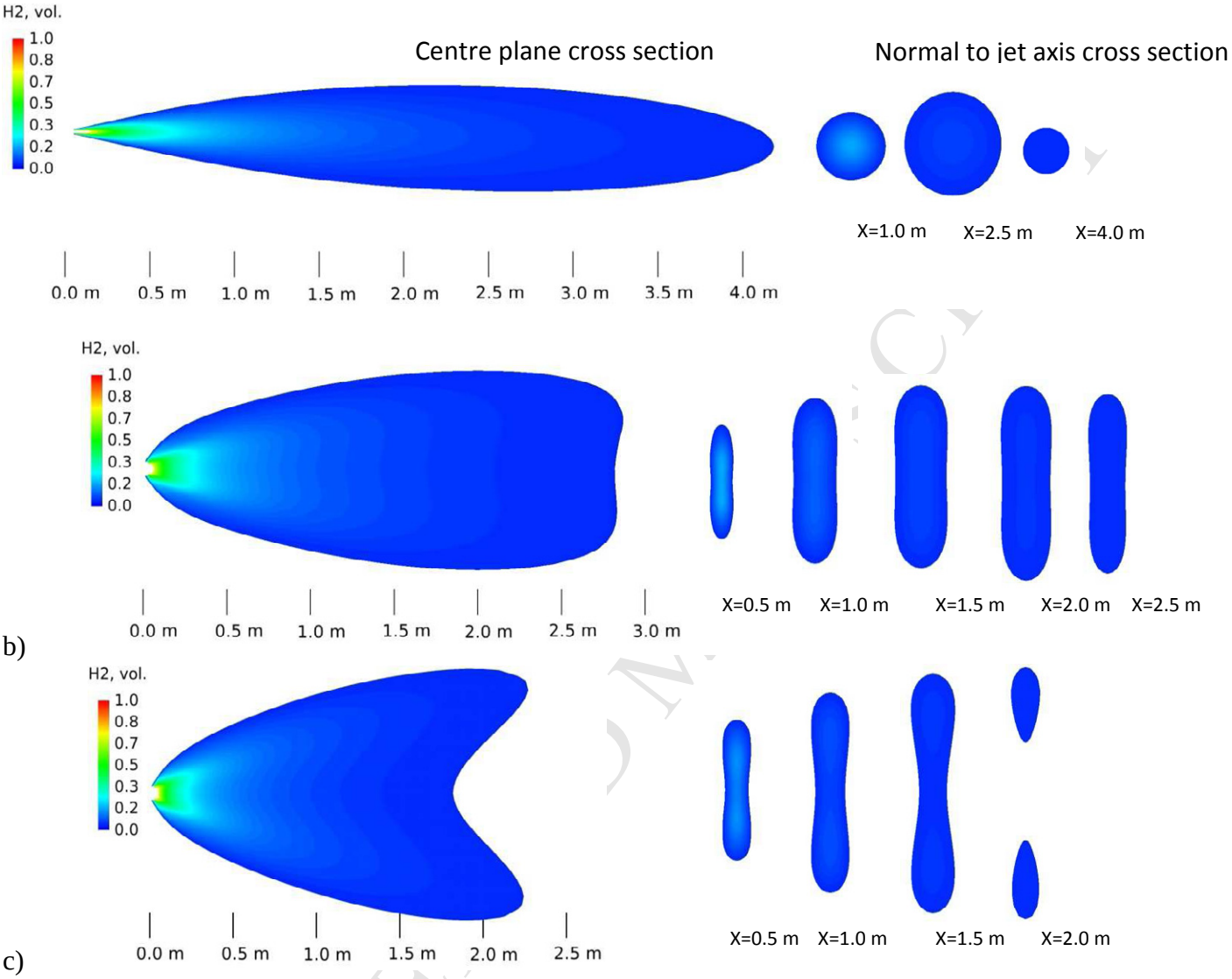
H2, vol.
1.0
0.8
0.7
0.5
0.3
0.2
0.0
Centre plane cross section
Normal to jet axis cross section
X=1.0 m
X=2.5 m
X=4.0 m
0.0 m
0.5 m
1.0 m
1.5 m
2.0 m
2.5 m
3.0 m
3.5 m
4.0 m
b)
H2, vol.
1.0
0.8
0.7
0.5
0.3
0.2
0.0
X=0.5 m
X=1.0 m
X=1.5 m
X=2.0 m
X=2.5 m
0.0 m
0.5 m
1.0 m
1.5 m
2.0 m
2.5 m
3.0 m
c)
H2, vol.
1.0
0.8
0.7
0.5
0.3
0.2
0.0
X=0.5 m
X=1.0 m
X=1.5 m
X=2.0 m
0.0 m
0.5 m
1.0 m
1.5 m
2.0 m
2.5 m

Figure 3

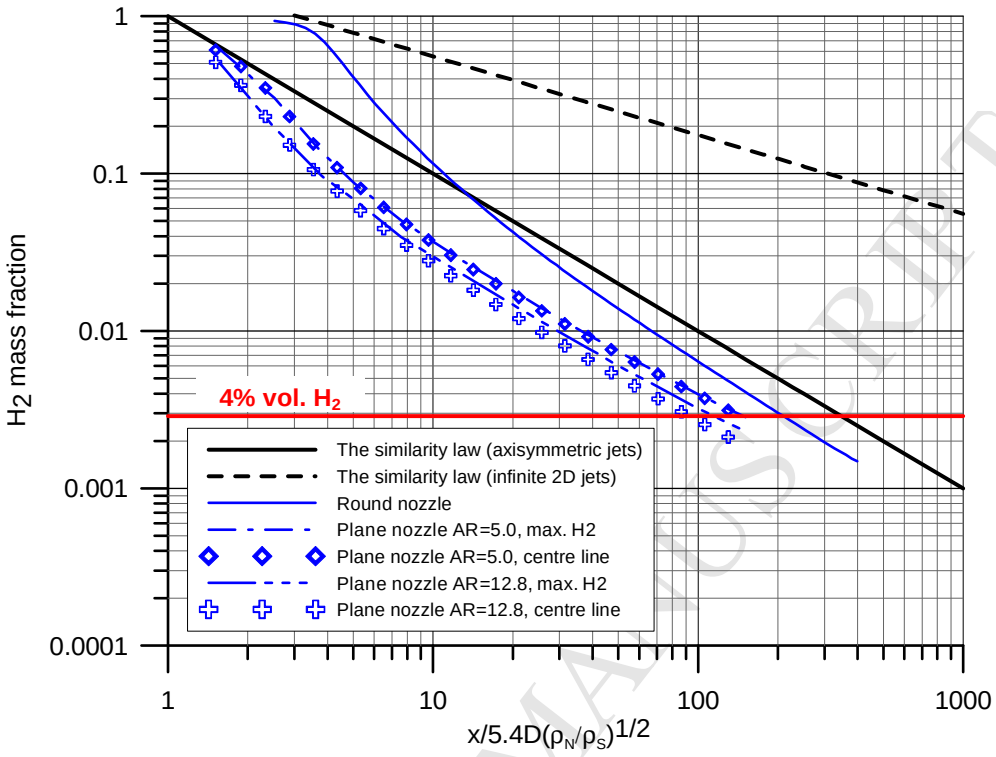

Figure 4

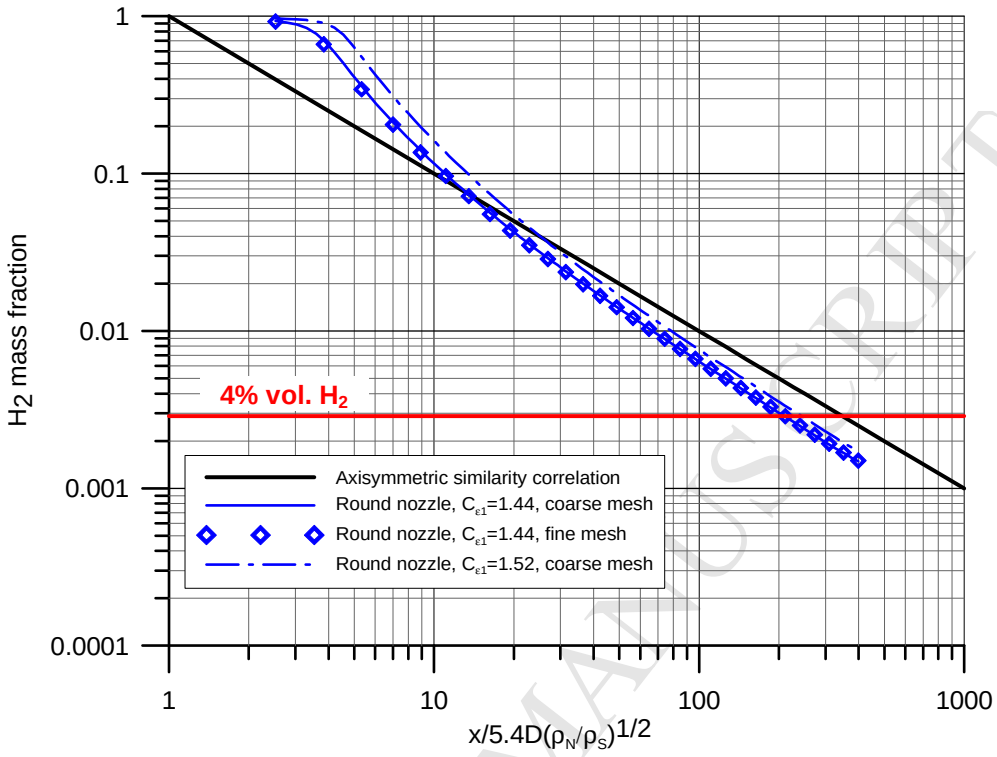

Figure 5

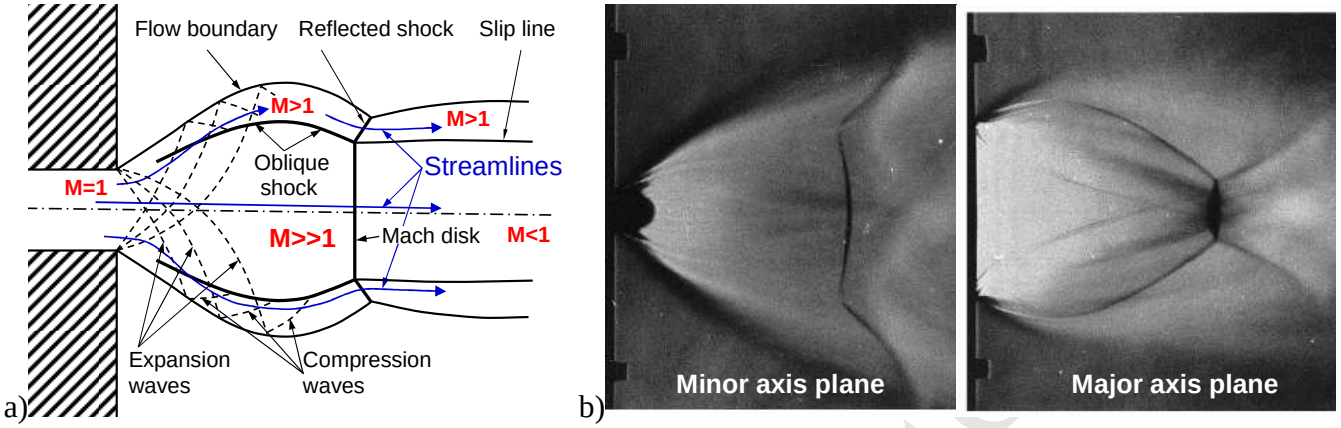

Figure 6

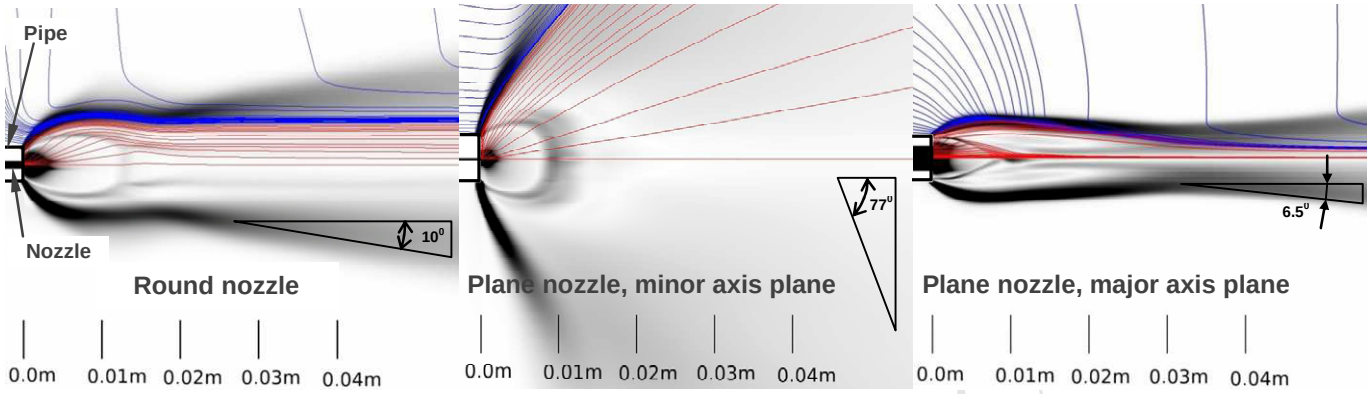

Figure 7

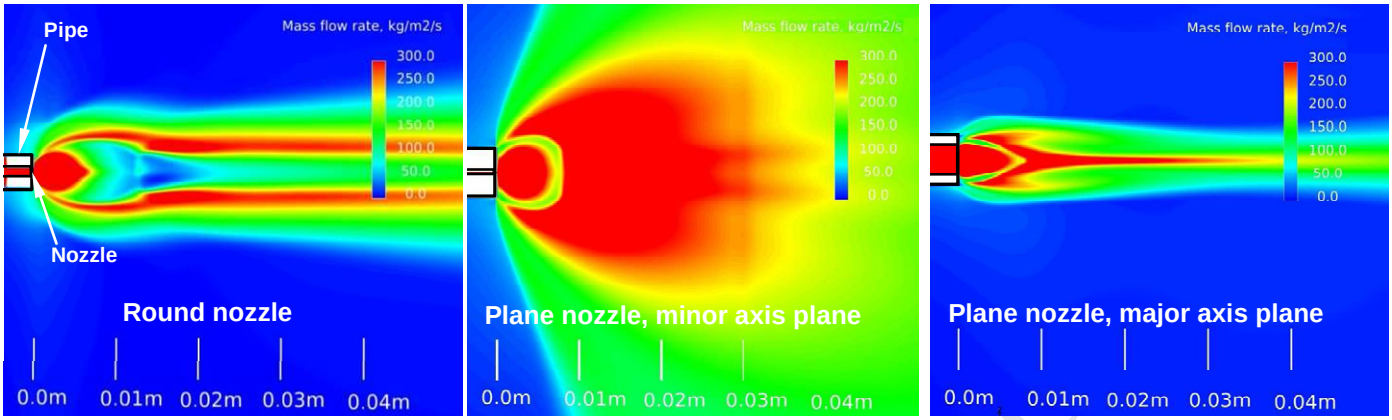

Figure 8

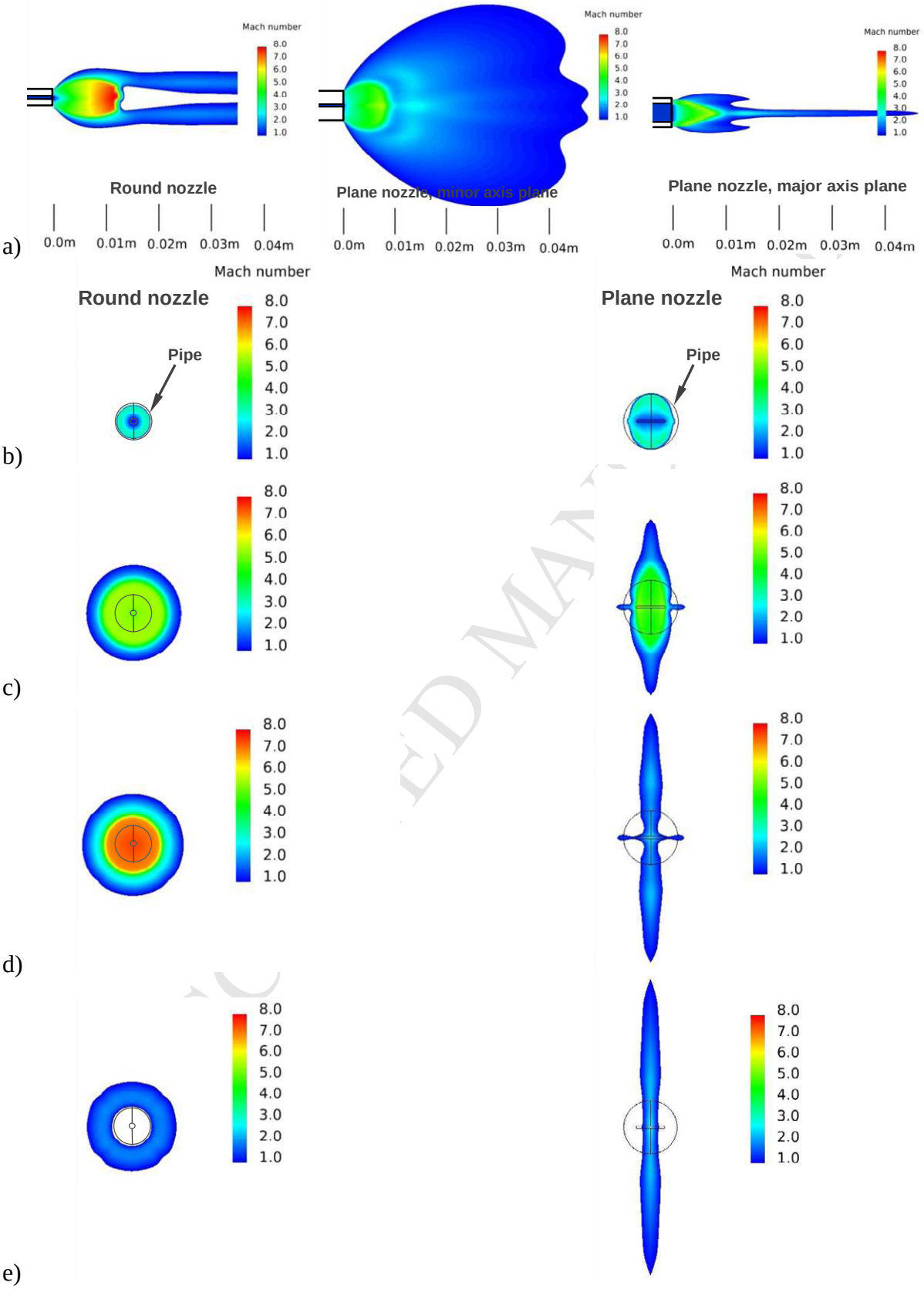
a)
Mach number
8.0
7.0
6.0
5.0
4.0
3.0
2.0
1.0
Round nozzle
Plane nozzle, minor axis plane
Plane nozzle, major axis plane
0.0m
0.01m
0.02m
0.03m
0.04m
b)
Round nozzle
Plane nozzle
Pipe
c)
d)
e)

Figure 9

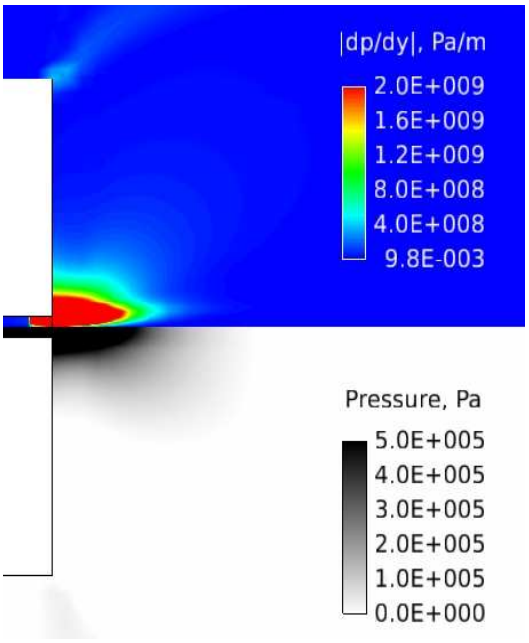

a)

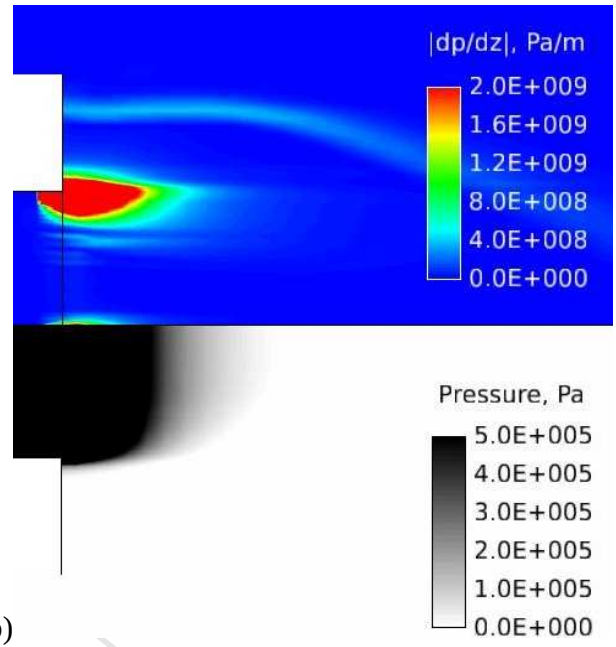

b)

Figure 10

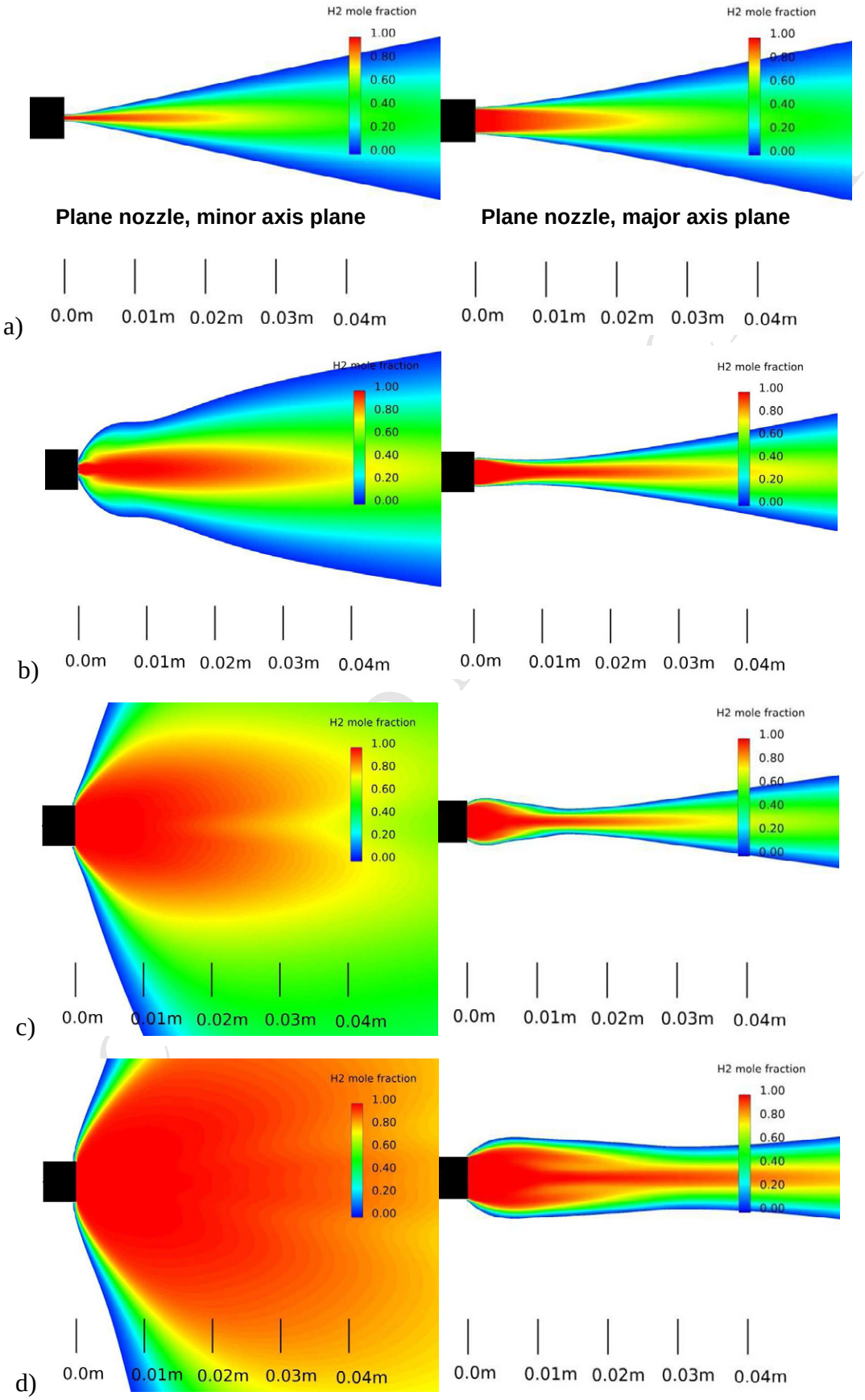
H2 mole fraction
1.00
0.80
0.60
0.40
0.20
0.00
Plane nozzle, minor axis plane
Plane nozzle, major axis plane
a)
b)
c)
d)
0.0m
0.01m
0.02m
0.03m
0.04m

Figure 11

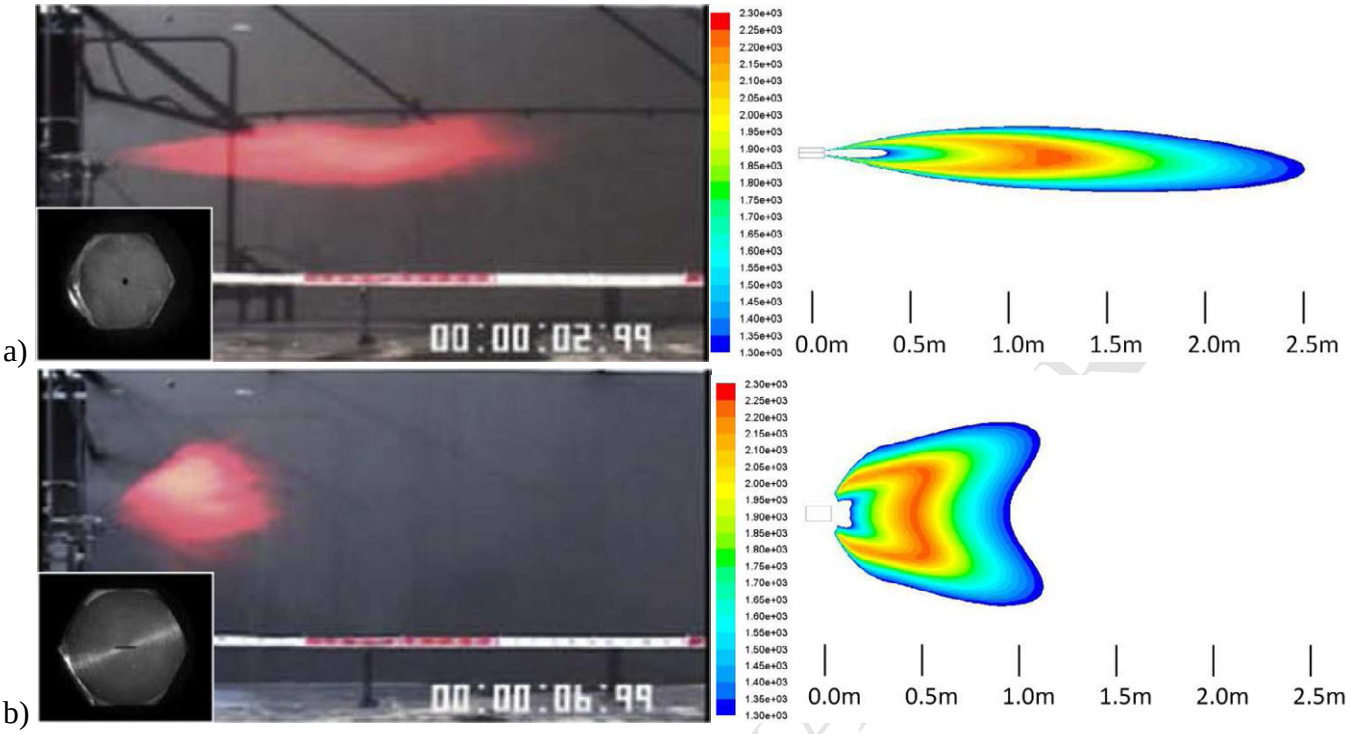

Figure 12

a) 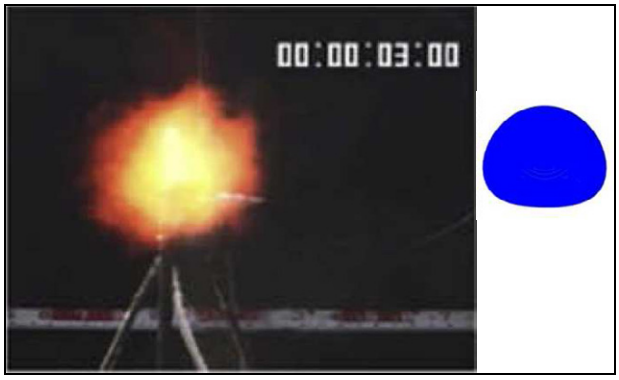

b) 

Tables

Table 1. Values of numerical parameters controlled at the outflow/inflow interface between compressible/incompressible domains, and their relative error Δε (non-reacting jet simulations).

Nozzle and boundary type		H_2 mass flow rate, kg/s	Δε, %	Impulse, kg·m/s^2	Δε, %	Max H_2 mass fraction, -	Δε, %	Max velocity, m/s	Δε, %
Round	Outflow	0.0156	1.28	31.1	2.89	0.9405	1.75	1534.5	1.83
	Inflow	0.0154		30.2		0.9246		1506.4	
AR5.0	Outflow	0.0152*	1.32	15.72	0.70	0.6240	0.05	1375.9	0.01
	Inflow	0.0150*		15.61		0.6237		1375.7	
AR12.8	Outflow	0.0136*	1.47	14.46	1.80	0.5216	2.93	1248.5	2.94
	Inflow	0.0134*		14.20		0.5063		1211.8	

Note: * - simulations were performed in a half of the real geometry, and by this reason the mass flow rate shown in Table 1 is multiplied by 2.

Highlights

- Circular and plane (aspect ratios 5.0 and 12.8) underexpanded hydrogen jets were simulated;
- Axis switching phenomena was studied for a range of storage pressures 0.5-40 MPa;
- Axis switch for underexpanded plane jet develops due to pressure gradient distribution around nozzle exit;
- Flattened jet profile was develop after axis switch and retained at least down to low flammability limit;
- Larger entrainment rate associated with plane jets provided smaller size of flammable envelope.